Prescribed-Time Three-Dimensional Guidance for Maneuvering Targets With Field-of-View and Approach Angle Constraints

Honglong Kang, Pengyu Wang, Shenmin Song, Robert Fonod

***Abstract*—This paper presents a three-dimensional (3D) guidance law for homing missiles to intercept maneuvering targets, while ensuring a desired final approach angle and satisfying field-of-view (FOV) constraints. First, a line-of-sight (LOS) vector shaping method is introduced in the range domain. The desired approach angle and FOV constraint can be satisfied by precisely tracking a specified LOS vector profile. Then, a feedback guidance law is designed using a prescribed-time control technique for nullifying the LOS tracking errors. This guidance law employs an extended state observer to estimate and compensate for unknown target maneuvers, with a rigorous analysis conducted to ensure the stability of the entire system. Unlike existing studies, the proposed guidance law does not require linearization procedures and switching logic, which avoids discontinuous guidance command and facilitates practical implementation. Finally, extensive numerical simulations and comparison studies validate the effectiveness, robustness, and superiority of the proposed method.**

***Index Terms*—Three-dimensional (3D) guidance, maneuvering target, approach angle control, field-of-view (FOV) constraint, line-of-sight (LOS) vector shaping.**

I. Introduction

Homing guidance systems with specific constraints, such as approaching the target with desired LOS angles and satisfying the FOV constraint, have attracted considerable attention in recent years due to their significance in practical applications. In particular, the approach angle control guidance is able to guide the missile to avoid terrain obstacles and increase the warhead effectiveness. The FOV constraint can confine the lead angle of the missile to ensure the onboard seeker remains locked onto the target. These two constraints sometimes need to be met simultaneously to enhance guidance effectiveness, leading to a more complex research problem: FOV-limited approach angle control guidance.

Numerous research efforts have focused on developing approach angle control guidance laws. One of the pioneering studies was presented in [1], in which the desired approach angle was achieved by solving a time-to-go weighted optimal guidance problem. Subsequently, various technical methods were applied in designing approach angle control guidance laws, such as biased proportional navigation guidance (PNG) [2], [3], trajectory shaping [4], and optimal control [5]. Two auxiliary functions were employed in [6] to construct a look angle profile and then meet the terminal constraints via a feedback guidance law. A generalized inversion guidance method was presented in [7], where an accurate time-to-go solution was developed under the approach angle constraint. However, it should be noted that the approach angle control guidance laws in [1]–[7] are only effective for stationary targets.

Designing a guidance law for maneuvering targets is generally a challenging task, especially when it needs to satisfy the approach angle constraint. In this regard, an explicit time-to-go prediction was used in [8] to drive an approach angle control guidance law for capturing maneuvering targets. The maximum bound of the unknown target maneuver was compensated in [9] by an adaptive law to achieve the desired approach angle. In [10], an integral sliding mode guidance law against maneuvering targets was developed by combining a time-to-go weighted error dynamic. For the 3D approach angle control problem, a range of methodologies have been implemented in existing research, including adaptive twisting control [11], incremental dynamic inversion method [12], model predictive control [13], and event-triggered control [14]. In [15], a quaternion-based approach angle control guidance law was derived in 3D space without model decoupling.

The FOV constraint is essential for practical implementation, as curved missile trajectories may cause the seeker to lose the target. In [16], [17], a switching logic was used to design FOV-limited guidance laws that ensure the missile lead angle does not exceed its maximum permissible value. The guidance command in [18] switched from a deviated pursuit phase to a PNG phase to satisfy the FOV constraint. However, the use of switching logic may lead to discontinuous commands and undesired chattering, which could potentially degrade the accuracy of the guidance system in practice. To this end, lead angle tracking method and trajectory shaping guidance were developed in [19]–[23] for satisfying the FOV constraint with smooth guidance commands. Based on trigonometric series, a FOV-limited guidance law was derived in [24] using the convex quadratic programming algorithm. It is noteworthy that the trajectory generated in [24] was infinitely differentiable. After that, a trajectory optimization problem determining the minimum wind strength was solved in [25] to analyze the performance of dynamic soaring, where a control vector was formulated smoothly by trigonometric series.

Few existing studies simultaneously address both approach angle control and FOV constraints in the presence of maneuvering targets. The sliding mode control and backstepping strategies were employed in [26]–[28] to design nonlinear guidance laws. Nevertheless, the nonlinear nature of such guidance laws makes it challenging to obtain an achievable region analytically. In [29], an achievable approach angle region was derived for maneuvering targets and the FOV

(Corresponding author: Pengyu Wang)

Honglong Kang and Shenmin Song are with the Center for Control Theory and Guidance Technology, Harbin Institute of Technology, Harbin 150001, China. (e-mail: kanghonglong@stu.hit.edu.cn; songshenmin@hit.edu.cn)

Pengyu Wang is with the Department of Control Science and Engineering, Harbin Institute of Technology, Harbin 150001, China. (e-mail: wangpy_hit@163.com)

Robert Fonod is with the School of Architecture, Civil and Environmental Engineering, École Polytechnique Fédérale de Lausanne, Lausanne CH-1015, Switzerland. (e-mail: robert.fonod@ieee.org)

constraint was met in 2D space. Note that the aforementioned 2D FOV-limited guidance laws [26]–[29] are not applicable to 3D scenarios. More recently, two 3D FOV-limited guidance laws were presented in [30], [31] by decoupling the 3D kinematics model. In [30], a 3D back-stepping guidance law was proposed to satisfy the FOV constraint, in which the engagement geometry was decoupled into two separate orthogonal planes. In [31], a 3D FOV-limited guidance law was designed for intercepting a constant speed target, wherein the LOS angles in yaw and pitch planes were shaped separately. It should be mentioned that ignoring the coupling effects of the 3D engagement geometry may degrade the performance of the guidance law.

The vector guidance is exerted in this paper to tackle the 3D guidance problem due to its concise expression. In recent years, the vector guidance has been extensively implemented as a unified framework in both 2D and 3D space [32]–[41]. In [32] and [33], the final velocity direction of the missile under the PNG law was predicted and applied to the design of approach angle control guidance laws. A reference frame attached to a maneuvering target was introduced in [34] and [35] to solve the approach angle control guidance problem. In [36], a biased PNG law with a constant relative speed for intercepting a maneuvering target was developed, where the desired impact time was achieved via a computational scheme. In [37] and [38], the 3D approach angle control guidance law was decoupled into augmented plane guidance and trajectory shaping guidance. Moreover, desired approach angles were realized by 3D vector guidance laws in [39] and [40], where the missile speed variation was considered by integrating numerical iterations. Additionally, to obtain an analytical solution of the lead angle, a prescribed performance guidance law with FOV constraints was designed in [41].

Despite advancements in previous studies, the 3D approach angle control guidance law for capturing maneuvering targets still faces some unresolved issues, especially when the FOV constraint is considered. First, most existing approach angle control guidance laws were developed for stationary targets [1]–[7], [17]–[23], [32], [33], [37]. Directly applying these guidance laws to maneuvering targets may result in the violation of FOV constraints or terminal guidance command singularities. For maneuvering targets, several FOV-limited approach angle control guidance laws have been presented for 2D scenarios [26]–[29]. However, designing 3D guidance laws that simultaneously meet both approach angle and FOV constraints for maneuvering targets still demands further investigation. Second, previous studies have commonly used switching logic [16]–[18], [40] and nonlinear auxiliary functions [19], [22], [28], [29] to achieve FOV constraints. Guidance laws based on switching logic may cause undesired chattering or discontinuous guidance commands, which degrade the accuracy of the guidance system. While guidance laws using auxiliary functions avoid model switching, their achievable region is difficult to determine due to the non-integrability of the auxiliary functions.

In light of all the technical issues discussed above, this paper introduces a FOV-limited guidance law for the 3D approach angle control, in which a prescribed-time ESO is used to estimate the perturbation term caused by maneuvering targets. The main contributions include:

1) Formulating the 3D guidance model between the missile and the target in a relative coordinate system, in which the FOV constraint is specifically transformed into a limit on the relative lead angle, rather than the original lead angle.
2) Developing a LOS vector shaping method using Rodrigues' rotation formula to realize approach angle and FOV constraints by accurately tracking the desired LOS vector.
3) Estimating target maneuvers using a prescribed-time ESO, and developing a feedback guidance law based on sliding-mode control technique with rigorous stability analysis.
4) Obtaining the analytical achievable region of the approach angle and the maximum permissible FOV constraint value for practical guidance implementation.

This paper is organized as follows. Section II presents the 3D guidance geometry against a maneuvering target and the guidance objectives. Section III describes the LOS shaping method with feasible analysis. Section IV proposes the feedback guidance law and analyzes prescribed-time stability. Section V validates the guidance law's performance.

II. Problem Statement

A. Guidance Model in Inertial Coordinate System

The 3D guidance geometry between a missile and a maneuvering target is depicted in Fig. 1, where (X_I, Y_I, Z_I) is the Cartesian inertial coordinate system. The missile and target velocities are expressed by $\boldsymbol{V}_M$ and $\boldsymbol{V}_T$, respectively. The LOS vector $\boldsymbol{R}$ represents the target's position relative to the missile. The elevation and azimuth LOS angles are denoted by θ_L and ϕ_L, respectively. The included angle between vectors $\boldsymbol{V}_M$ and $\boldsymbol{R}$ is defined as the total lead angle of the missile, which is denoted as σ_M.

In this paper, the notations $\boldsymbol{v}_M$, $\boldsymbol{v}_T$ and $\boldsymbol{r}$ stand for the unit vectors along $\boldsymbol{V}_M$, $\boldsymbol{V}_T$, and $\boldsymbol{R}$, respectively. That is

$$\boldsymbol{v}_M = \frac{\boldsymbol{V}_M}{V_M}, \quad \boldsymbol{v}_T = \frac{\boldsymbol{V}_T}{V_T}, \quad \boldsymbol{r} = \frac{\boldsymbol{R}}{R} \tag{1}$$

where $R = ||\boldsymbol{R}||$, $V_M = ||\boldsymbol{V}_M||$, and $V_T = ||\boldsymbol{V}_T||$. Like most of previous studies, we also assume that the missile speed V_M and the target speed V_T remain constant throughout the entire guidance procedure.

Under the inertial coordinate system in Fig. 1, the guidance model between the missile and target can be given as

$$\dot{R} = (\boldsymbol{V}_T - \boldsymbol{V}_M) \cdot \boldsymbol{r}, \tag{2}$$

$$\dot{\boldsymbol{r}} = \frac{[\boldsymbol{r} \times (\boldsymbol{V}_T - \boldsymbol{V}_M)] \times \boldsymbol{r}}{R}, \tag{3}$$

$$\dot{\boldsymbol{v}}_M = \frac{\boldsymbol{A}_M}{V_M}, \quad \dot{\boldsymbol{v}}_T = \frac{\boldsymbol{A}_T}{V_T} \tag{4}$$

where vectors $\boldsymbol{A}_M$ and $\boldsymbol{A}_T$ are the lateral control accelerations acting on the missile and target, respectively.

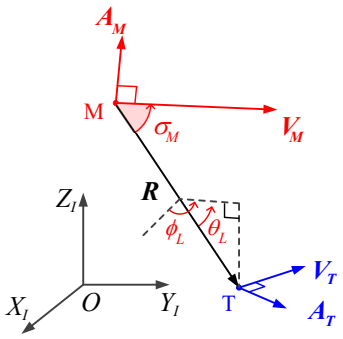

Fig. 1: Guidance geometry in inertial coordinate system.

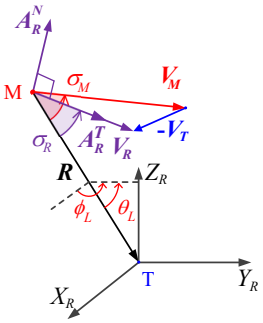

Fig. 2: Guidance geometry in relative coordinate system.

B. Guidance Model in Relative Coordinate System

Now, as shown in Fig. 2, we introduce a relative coordinate system (X_R, Y_R, Z_R) with its origin fixed on the target. The relative velocity can be expressed as

$$\boldsymbol{V}_R = \boldsymbol{V}_M - \boldsymbol{V}_T. \tag{5}$$

A unit vector along the relative velocity is defined as $\boldsymbol{v}_R = \boldsymbol{V}_R/V_R$ where $V_R = ||\boldsymbol{V}_R||$ is the relative speed between the missile and target, which is not a constant. Differentiating $\boldsymbol{V}_R$ with respect to time yields

$$\dot{\boldsymbol{V}}_R = \dot{\boldsymbol{V}}_M - \dot{\boldsymbol{V}}_T = \boldsymbol{A}_M - \boldsymbol{A}_T = \underbrace{\dot{V}_R \boldsymbol{v}_R}_{\boldsymbol{A}_R^T} + \underbrace{V_R \dot{\boldsymbol{v}}_R}_{\boldsymbol{A}_R^N} \tag{6}$$

where $\boldsymbol{A}_R^T$ denotes the tangential acceleration and $\boldsymbol{A}_R^N$ stands for the lateral acceleration. In this paper, $\boldsymbol{A}_R^N$ will serve as the control input in the subsequent guidance law design.

Under the relative coordinate system in Fig. 2, the guidance model (2)–(4) can be rewritten as

$$\dot{R} = -\boldsymbol{V}_R \cdot \boldsymbol{r}, \tag{7}$$

$$\dot{\boldsymbol{r}} = \boldsymbol{\Omega}_L \times \boldsymbol{r}, \tag{8}$$

$$\dot{\boldsymbol{v}}_R = \boldsymbol{\Omega}_{V_R} \times \boldsymbol{v}_R = \boldsymbol{A}_R^N / V_R \tag{9}$$

where vectors $\boldsymbol{\Omega}_L$ and $\boldsymbol{\Omega}_{V_R}$ are the rotation rates of the LOS $\boldsymbol{R}$ and the relative velocity $\boldsymbol{V}_R$, respectively, which can be expressed as

$$\boldsymbol{\Omega}_L = -\frac{\boldsymbol{r} \times \boldsymbol{V}_R}{R}, \quad \boldsymbol{\Omega}_{V_R} = \frac{\boldsymbol{V}_R \times \boldsymbol{A}_R}{V_R^2}. \tag{10}$$

Furthermore, the relative lead angle, i.e., the included angle between $\boldsymbol{V}_R$ and $\boldsymbol{R}$, is defined as σ_R. According to geometric relations in Fig. 2, one has

$$\cos\sigma_R = \boldsymbol{r} \cdot \boldsymbol{v}_R, \tag{11}$$

$$\sin\sigma_R \boldsymbol{k}_R = \boldsymbol{r} \times \boldsymbol{v}_R \tag{12}$$

where $\boldsymbol{k}_R = \boldsymbol{r} \times \boldsymbol{v}_R / ||\boldsymbol{r} \times \boldsymbol{v}_R||$ is a unit normal vector. Taking the time derivative of (11), we obtain

$$\dot{\sigma}_R = (\boldsymbol{\Omega}_{V_R} - \boldsymbol{\Omega}_L) \cdot \boldsymbol{k}_R. \tag{13}$$

Then the dynamic of $\boldsymbol{\Omega}_L$ can be derived as:

$$\dot{\boldsymbol{\Omega}}_L = -2\frac{\dot{R}}{R}\boldsymbol{\Omega}_L + \frac{\dot{R}}{R}\boldsymbol{\Omega}_{V_R} + \boldsymbol{D} \tag{14}$$

where $\boldsymbol{D} = \boldsymbol{A}_R^T \times \boldsymbol{r}/R$ is the perturbation term caused by the target maneuvers.

C. Guidance Objectives

This paper aims to meet the following guidance objectives:

1) *Zero miss distance*: The missile should successfully intercept the target, i.e., $R \to 0$.

2) *FOV constraint*: The FOV angle should be constrained within its upper bound. Ignoring the angle of attack and side-slip angle, the FOV constraint can be approximated as

$$|\sigma_M| < \sigma_M^{\max} \tag{15}$$

where $\sigma_M^{\max}$ is the maximum permissible value of σ_M.

3) *Desired approach angles*: The missile needs to achieve desired LOS angles at the final moment. That is, $\theta_L \to \theta_{Lf}$ and $\phi_L \to \phi_{Lf}$, where θ_{Lf} and ϕ_{Lf} are the desired elevation and azimuth LOS angles. We define a desired unit vector $\boldsymbol{r}_f$ as follows:

$$\boldsymbol{r}_f = [\cos\phi_{Lf}\cos\theta_{Lf}, \sin\phi_{Lf}\cos\theta_{Lf}, \sin\theta_{Lf}]. \tag{16}$$

It is obvious that if $\boldsymbol{r} = \boldsymbol{r}_f$ at the final moment, the desired approach angles are achieved. Therefore, the last guidance objective of this paper is to ensure $\boldsymbol{r} \to \boldsymbol{r}_f$.

Remark 1: The approach angle control problem with FOV constraints is said to be challenging even under the assumption that the speeds of the missile and target are constant. First, the achievable region of the approach angle is related to the maximum permissible value of the relative lead angle. In general, it is difficult to obtain an explicit mathematical relation between the approach angle region and the FOV constraint, particularly in 3D scenarios. Second, the unknown maneuvers may result in the target escaping from the detectable region of the seeker, hence it is necessary to compensate the disturbances caused by the targets in the guidance law design.

We present the following lemma as a sufficient condition for FOV constraints and its proof is provided in Appendix A.

Lemma 1: Considering the guidance model (7)–(10), if the relative lead angle always satisfies $|\sigma_R| \le \sigma_R^{\max}$ where $\sigma_R^{\max}$ is the maximum permissible value of σ_R:

$$\sigma_R^{\max} = \operatorname{asin}\left(\frac{\sin\sigma_M^{\max} - \rho_M}{1 + \rho_M}\right) \tag{17}$$

and asin() is the arcsin function, $\rho_M = V_T/V_M$ is assumed to meet $\rho_M < \sin\sigma_M^{\max}$, then the missile can achieve the FOV constraint.

Remark 2: The advantage of Lemma 1 is illustrated in this remark. Under most existing FOV-limited guidnace laws for stationary targets, the FOV constraint is typically satisfied during the entire guidance procedure. However, the guidance system may operate with a large lead angle very close to the upper boundary. This increases the risk of violating the FOV constraint, especially when the target is maneuvering. In this paper, the actual maximum value of FOV is always smaller than the specified maximum permissible value $\sigma_M^{\max}$, as indicated in Lemma 1. In other words, there will be safety margins between the peak values of lead angle and the upper bounds of lead angle. This property is considered an advantage of this paper.

III. LOS Vector Shaping Method

In this section, a LOS vector shaping method is proposed for the FOV-limited approach angle control guidance problem. First, a unit LOS vector profile is constructed using Rodrigues' rotation formula. The approach angle and FOV constraints can be achieved as long as the LOS vector profile is tracked precisely by the missile. Then, the behavior of the lead angle under the proposed method is rigorously analyzed without any linearization procedures. In particular, the mathematical relationship between the maximum permissible FOV constraint and the approach angle is derived analytically, leading to an achievable region that facilitates practical implementation.

A. Design of LOS Vector Shaping Method

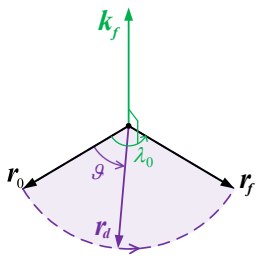

Fig. 3: Unit LOS vector rotation in 3D space.

The unit LOS vector rotation geometry is depicted in Fig. 3. The unit vector $\boldsymbol{k}_f$ represents the rotation axis determined by the initial unit LOS vector $\boldsymbol{r}_0$ and the desired unit LOS vector $\boldsymbol{r}_f$. From Fig. 3 one can obtain

$$\cos\lambda_0 = \boldsymbol{r}_f \cdot \boldsymbol{r}_0, \tag{18}$$

$$\sin\lambda_0 \boldsymbol{k}_f = \boldsymbol{r}_f \times \boldsymbol{r}_0 \tag{19}$$

where λ_0 is the initial approach angle error, i.e., the included angle between $\boldsymbol{r}_0$ and $\boldsymbol{r}_f$.

Define $\tau = R/R_0$ where R_0 is the initial relative range. In this paper, the unit LOS vector profile is formulated as

$$\boldsymbol{r}_d = \boldsymbol{r}_0\cos\vartheta + \boldsymbol{k}_f \times \boldsymbol{r}_0 \sin(-\vartheta) \tag{20}$$

where ϑ is a rotation variable, as depicted in Fig. 3. We design the rotation variable ϑ as

$$\vartheta = \lambda_0\left[1 - \operatorname{atan}(\beta\tau^n)/\operatorname{atan}\beta\right] \tag{21}$$

where atan() is the arctangent function, λ_0 is the initial approach angle error, $n \geq 2$ and $\beta > 1$ are tuning parameters. It is easy to verify that $\vartheta = 0$ when $R = R_0$.

The LOS vector profile $\boldsymbol{r}_d$ will gradually rotate from $\boldsymbol{r}_0$ to the final desired unit vector $\boldsymbol{r}_f$ throughout the guidance duration, as will be shown in the following theorem.

Theorem 1: For the guidance model (7)–(10), if the profile (20) is precisely tracked by the missile and the tuning parameters satisfies

$$\frac{n}{\operatorname{atan}\beta} < \frac{2}{\lambda_0}\tan\sigma_R^{\max}, \tag{22}$$

then the zero miss distance, FOV constraint, and desired approach angles can be achieved with bounded terminal acceleration command.

Proof : Differentiating (20) with respect to time, we have

$$\dot{\boldsymbol{r}}_d = -\dot{\vartheta}\left(\boldsymbol{r}_0\sin\vartheta + \boldsymbol{k}_f \times \boldsymbol{r}_0\cos\vartheta\right). \tag{23}$$

Combining (10) with (12), the angular velocity of LOS can be expressed as

$$\boldsymbol{\Omega}_L = -\frac{V_R}{R}\sin\sigma_R \boldsymbol{k}_R. \tag{24}$$

Note that Theorem 1 gives $\boldsymbol{r} = \boldsymbol{r}_d$ during the guidance process. Substituting (20) and (23) into (8) yields

$$\begin{aligned}\boldsymbol{\Omega}_L &= -\dot{\vartheta}(\boldsymbol{r}_0\cos\vartheta + \boldsymbol{k}_f \times \boldsymbol{r}_0\sin(-\vartheta)) \\ &\quad \times (\boldsymbol{r}_0\sin\vartheta + \boldsymbol{k}_f \times \boldsymbol{r}_0\cos\vartheta) \\ &= \dot{\vartheta}(\boldsymbol{k}_f \times \boldsymbol{r}_0) \times \boldsymbol{r}_0 = -\dot{\vartheta}\boldsymbol{k}_f.\end{aligned} \tag{25}$$

From (24) and (25), one can deduce that

$$\dot{\vartheta} = \frac{V_R}{R}\sin\sigma_R. \tag{26}$$

The above equation can be rearranged as

$$\tan\sigma_R = -R\frac{d\vartheta}{dR}. \tag{27}$$

For notational simplicity, let $\omega = \lambda_0/\operatorname{atan}\beta$. Differentiating (21) with respect to R, we obtain

$$\frac{d\vartheta}{dR} = -n\frac{\omega}{R_0}\frac{\beta\tau^{n-1}}{1+\beta^2\tau^{2n}} < 0. \tag{28}$$

It is obvious that $\tan\sigma_R > 0$ and $\sigma_R \in [0, \pi/2)$ are satisfied during the guidance procedure, thus R will monotonically decrease to zero. According to $\vartheta(R=0) = \lambda_0$,

$$\begin{aligned}\lim_{R\to 0}\boldsymbol{r}_d &= \boldsymbol{r}_0\cos\lambda_0 + \boldsymbol{k}_f \times \boldsymbol{r}_0\sin(-\lambda_0) \\ &= \boldsymbol{r}_0\cos\lambda_0 + \boldsymbol{r}_0 \times (\boldsymbol{r}_f \times \boldsymbol{r}_0).\end{aligned} \tag{29}$$

The use of triple product rules gives

$$\begin{aligned}\lim_{R\to 0}\boldsymbol{r}_d &= \boldsymbol{r}_0\cos\lambda_0 + (\boldsymbol{r}_0\cdot\boldsymbol{r}_0)\boldsymbol{r}_f - (\boldsymbol{r}_0\cdot\boldsymbol{r}_f)\boldsymbol{r}_0 \\ &= \boldsymbol{r}_0\cos\lambda_0 + \boldsymbol{r}_f - \boldsymbol{r}_0\cos\lambda_0 = \boldsymbol{r}_f\end{aligned} \tag{30}$$

which implies that the zero miss distance and desired approach angles can be achieved. Substituting (28) into (27) yields

$$\tan\sigma_R = n\omega\frac{\beta\tau^n}{1+\beta^2\tau^{2n}}. \tag{31}$$

Taking the derivative of (31) with respect to R, we obtain

$$\frac{d\sigma_R}{dR} = n^2 \frac{\omega}{R_0} \frac{\beta(1-\beta^2\tau^{2n})}{(1+\beta^2\tau^{2n})^2}(1+\sigma_R^2)\tau^{n-1}. \tag{32}$$

We denote the right-hand side of (31) as $F(R)$, then we have

$$\frac{dF(R)}{dR} = n^2 \frac{\omega}{R_0} \frac{(1-\beta^2\tau^{2n})\beta}{(1+\beta^2\tau^{2n})^2}\tau^{n-1}. \tag{33}$$

According to (28), one can deduce that τ decreases monotonically from 1 to 0. Then the behavior of $F(R)$ and σ_R in the range domain can be analyzed using (33) as follows:

1) $dF(R)/dR < 0$ and $d\sigma_R/dR < 0$ when $\tau \in (\beta^{-1/n}, 1)$.
2) $dF(R)/dR = 0$ and $d\sigma_R/dR = 0$ when $\tau = \beta^{-1/n}$.
3) $dF(R)/dR > 0$ and $d\sigma_R/dR > 0$ when $\tau \in (0, \beta^{-1/n})$.

This indicates that the relative lead angle monotonically increases when $\beta^{-1/n}R_0 < R < R_0$ and then decreases when $0 < R < \beta^{-1/n}R_0$. As a result, the maximum relative lead angle can be predicted as

$$\tan\sigma_R^{\text{pre}} = F\left(\beta^{-1/n}R_0\right) = \frac{n\lambda_0}{2\operatorname{atan}\beta} \tag{34}$$

where the variable with superscript "pre" refer to the predicted value. Combining (22) with (34) leads to $\sigma_R^{\text{pre}} < \sigma_R^{\max}$. Recalling Lemma 1 we can conclude that the lead angle will not violate its constraint.

Next, we analyze the property of terminal lead angle and terminal acceleration command. As $R \to 0$, (31) becomes

$$\begin{aligned}\lim_{R\to 0}\sigma_R &= \lim_{\tau\to 0}\operatorname{atan}\left(n\omega\frac{\beta\tau^n}{1+\beta^2\tau^{2n}}\right)\\ &= \operatorname{atan}\left(n\omega\beta\lim_{\tau\to 0}\frac{\tau^n}{1+\beta^2\tau^{2n}}\right) = 0.\end{aligned} \tag{35}$$

Clearly, a terminal relative lead angle of zero can be achieved. Using L'Hospital's rule, (24) gives

$$\lim_{R\to 0}\|\boldsymbol{\Omega}_L\| = V_{Rf}\lim_{R\to 0}\frac{\sin\sigma_R}{R} = V_{Rf}\lim_{R\to 0}\frac{\dot{\sigma}_R}{\dot{R}} \tag{36}$$

where V_{Rf} is the terminal relative speed. Substituting (32) into (36) leads to

$$\lim_{R\to 0}\|\boldsymbol{\Omega}_L\| = n^2\frac{\omega V_{Rf}}{R_0}\lim_{R\to 0}\tau^{n-1}. \tag{37}$$

Obviously, $\lim_{R\to 0}\|\boldsymbol{\Omega}_L\| = 0$ and bounded terminal acceleration command are guaranteed by choosing $n \geq 2$. This completes the proof. ∎

B. Analysis of LOS Vector Shaping Method

From (21) we can see that the behavior of rotation variable is determined by two parameters n and β. Based on Theorem 1, the conditions for parameters selection can be summarized as follows:

1) The selection of n should satisfy $n \geq 2$ to guarantee a bounded terminal acceleration command, as demonstrated in (37).
2) The choice of β should meet $\operatorname{atan}\beta > n\lambda_0/(2\tan\sigma_R^{\max})$ and $\beta > 1$ to achieve the FOV constraint, as indicated by (22) and (34).

An analytical achievable region is presented herein to further analysis the property of the proposed method. The mathematical relation between $\sigma_R^{\max}$ and the initial guidance error λ_0 can be rearrange as

$$\lambda_0 < \frac{2}{n}\operatorname{atan}\beta\tan\sigma_R^{\max} \tag{38}$$

which implies that a larger relative lead angle boundary $\sigma_R^{\max}$ will lead to a larger launch envelope. In other words, a larger λ_0 is permissible for approach angles control when a larger FOV boundary is selected.

Remark 3: This remark discusses the principles for establishing the rotational variable ϑ. The mathematical relationship (30) implies that the final approach angle is determined by $\vartheta(R = 0)$. According to (27), the relative lead angle is governed by $Rd\vartheta/dR$ under the proposed method. Thus the unified criterion for constructing ϑ can be summarized as

$$\vartheta(R=0) = \lambda_0, \quad R\frac{d\vartheta}{dR} \geq -\tan\sigma_R^{\max}. \tag{39}$$

Consequently, the formulation of the rotation variable ϑ is not unique, which means a variety of desired unit LOS vectors can be found to meet the guidance constraints. In [21], polynomial shaping was used to design a FOV-limited guidance law. Compared with [21], as various ϑ are feasible, our proposed method serves as a generalized tool for providing various guidance trajectories.

Remark 4: The proposed LOS vector shaping method may offer the following advantages.

1) The proposed method is derived rigorously using vector-form manipulation, without linearization or model decoupling. As a result, the guidance law remains effective in a sufficiently coupled engagement geometry.
2) Unlike most existing guidance laws, this paper formulates the achievable region of approach angles analytically. Therefore, the mission designer can select appropriate desired approach angles before implementing the guidance.
3) This paper eliminates the terminal singularity in the acceleration command, thereby enhancing the robustness and reliability of the guidance law during the terminal phase, particularly in the case of maneuvering targets.

At this point, we can draw the conclusion that for accomplishing the approach angle control with FOV constraints, the following requirements need to be fulfilled:

1) Proper construction of the unit LOS vector profile (20) by selecting the parameters under the condition (39).
2) Development of a guidance law enabling the missile to track the unit LOS vector profile precisely.

To satisfy these requirements, the sliding mode control technique and a predefined-time ESO are employed together in Section IV to derive an approach angle control guidance law with FOV constraints.

IV. Guidance Law Design

A feedback guidance law to track the LOS vector profile (20) is developed in this section by using the predefined-time control technique. The predefined-time stability of the

proposed guidance law is rigorously proven in the presence of unknown target maneuvers.

A. Predefined-Time Guidance Law

A scaling function for predefined-time convergence is introduced as follows

$$\mu(R,R_s)=\begin{cases}\dfrac{R_0-R_s}{R-R_s}, & t\in[0,t_s),\text{i.e., } R\in(R_s,R_0]\\ \mu_c, & t\in[t_s,t_f],\text{i.e., } R\in[0,R_s]\end{cases} \tag{40}$$

where μ_c is a design parameter, t_s is the specified settling time, and its value is determined by the specified settling range R_s.

For clarity, three scaling functions are designed as $\mu_i=\mu(R,R_{si}), i=1,2,3$ with $R_{s1}<R_{s2}<R_{s3}$ (i.e., $t_{s1}>t_{s2}>t_{s3}$). Note that in the following derivations, the three instants t_{s1},t_{s2},t_{s3} represent the convergence time of the tracking error, sliding surface, and the observation errors, respectively.

A tracking error e is defined as

$$\begin{aligned}\cos e&=\boldsymbol{r}_d\cdot\boldsymbol{r},\\ \sin e\boldsymbol{k}_d&=\boldsymbol{r}_d\times\boldsymbol{r}\end{aligned} \tag{41}$$

where $\boldsymbol{k}_d$ is a unit vector. It is obvious that $e=0$ only occurs when $\boldsymbol{r}=\boldsymbol{r}_d$. The tracking error dynamics can be derived as:

$$\begin{aligned}\dot{e}&=(\boldsymbol{\Omega}_L-\boldsymbol{\Omega}_{Ld})\cdot\boldsymbol{k}_d,\\ \dot{\boldsymbol{k}}_d&=\Omega_{\boldsymbol{k}_d}\times\boldsymbol{k}_d\end{aligned} \tag{42}$$

where $\boldsymbol{\Omega}_{\boldsymbol{k}_d}=\boldsymbol{\Omega}_L+\boldsymbol{\Omega}_{Ld}-(\boldsymbol{\Omega}_L-\boldsymbol{\Omega}_{Ld})\times\boldsymbol{k}_d\cot e$, $\boldsymbol{\Omega}_{Ld}=-\dot{\vartheta}\boldsymbol{k}_f$. The derivation of (42) is presented in Appendix B. In order to nullifying the tracking error e, a sliding surface is constructed as follows:

$$\boldsymbol{S}=(\boldsymbol{\Omega}_L-\boldsymbol{\Omega}_{Ld})+c_1\mu_1 e\boldsymbol{k}_d \tag{43}$$

where $c_1>0$ is a constant and μ_1 is a scaling function with a settling time t_{s1}. The time-derivative of $\boldsymbol{S}$ can be derived as

$$\dot{\boldsymbol{S}}=\boldsymbol{F}+\frac{\dot{R}}{R}\boldsymbol{\Omega}_{V_R}+\boldsymbol{D} \tag{44}$$

where $\boldsymbol{F}=-2\dot{R}/R\boldsymbol{\Omega}_L-\dot{\boldsymbol{\Omega}}_{Ld}+c_1(\dot{\mu}_1e\boldsymbol{k}_d+\mu_1\dot{e}\boldsymbol{k}_d+\mu_1e\dot{\boldsymbol{k}}_d)$. Then we propose the following guidance law:

$$\boldsymbol{\Omega}_{V_R}=\boldsymbol{\Omega}_{V_R}^{eq}+\boldsymbol{\Omega}_{V_R}^{sm}-\frac{R}{\dot{R}}\widehat{\boldsymbol{D}} \tag{45}$$

where $\boldsymbol{\Omega}_{V_R}^{eq}=-R/\dot{R}\boldsymbol{F}$, $\boldsymbol{\Omega}_{V_R}^{sm}=-R/\dot{R}(c_2\mu_2\boldsymbol{S}+c_3\mathbf{sign}(\boldsymbol{S}))$, μ_2 is a scaling function with a settling time t_{s2}; $\widehat{\boldsymbol{D}}$ is the observed value of $\boldsymbol{D}$.

In practice, it can be assumed that the perturbation term $\boldsymbol{D}$ and its derivative have upper bounds $\|\dot{\boldsymbol{D}}\|=\|\boldsymbol{\delta}\|\le\Delta$. Let $\widetilde{\boldsymbol{\Omega}}_L=\boldsymbol{\Omega}_L-\widehat{\boldsymbol{\Omega}}_L$ and $\widetilde{\boldsymbol{D}}=\boldsymbol{D}-\widehat{\boldsymbol{D}}$, where $\widehat{\boldsymbol{\Omega}}_L$ is the observed value of $\boldsymbol{\Omega}_L$. A predefined-time ESO is constructed as

$$\begin{aligned}\dot{\widehat{\boldsymbol{\Omega}}}_L&=-2\frac{\dot{R}}{R}\boldsymbol{\Omega}_L+\frac{\dot{R}}{R}\boldsymbol{\Omega}_{V_R}+\widehat{\boldsymbol{D}}+k_1\varpi\mu_3\widetilde{\boldsymbol{\Omega}}_L,\\ \dot{\widehat{\boldsymbol{D}}}&=k_2(\varpi\mu_3)^2\widetilde{\boldsymbol{\Omega}}_L\end{aligned} \tag{46}$$

where μ_3 is a scaling function with a settling time t_{s3}, and k_1,k_2,ϖ are positive observer gains. The closed-loop stability of the proposed guidance law is rigorously analyzed in the subsequent theorem.

Theorem 2: Under the guidance law (45) and the predefined-time ESO (46), the missile can precisely track the proposed LOS vector profile (20).

Proof : The proof of Theorem 2 is divided into two steps. The first step is the proof of convergence for the predefined-time ESO (46), and the second step is the proof of convergence for the tracking error (41).

Step 1 : Differentiating $\widetilde{\boldsymbol{\Omega}}_L$ and $\widetilde{\boldsymbol{D}}$ yields

$$\begin{aligned}\dot{\widetilde{\boldsymbol{\Omega}}}_L&=\widetilde{\boldsymbol{D}}-k_1\varpi\mu_3\widetilde{\boldsymbol{\Omega}}_L,\\ \dot{\widetilde{\boldsymbol{D}}}&=\boldsymbol{\delta}-k_2(\varpi\mu_3)^2\widetilde{\boldsymbol{\Omega}}_L.\end{aligned} \tag{47}$$

Let $\boldsymbol{\eta}=[\varpi\mu_3\widetilde{\boldsymbol{\Omega}}_L^T,\widetilde{\boldsymbol{D}}^T]^T$. Substituting (47) into the time derivative of $\boldsymbol{\eta}$ leads to

$$\dot{\boldsymbol{\eta}}=\varpi\mu_3\bar{\boldsymbol{A}}\boldsymbol{\eta}+\mu_3\bar{\boldsymbol{B}}\boldsymbol{\eta}+\boldsymbol{C} \tag{48}$$

where $\bar{\boldsymbol{A}}=\boldsymbol{A}\otimes\boldsymbol{I}_3,\bar{\boldsymbol{B}}=\boldsymbol{B}\otimes\boldsymbol{I}_3$, $\otimes$ denotes the Kronecker product, $\boldsymbol{C}=[0,0,0,\boldsymbol{\delta}^T]^T$, $\boldsymbol{I}_3$ is a three-dimensional identity matrix; $\boldsymbol{A}=\begin{bmatrix}-k_1 & 1\\ -k_2 & 0\end{bmatrix}$ and $\boldsymbol{B}=\begin{bmatrix}-\dot{R}/(R_0-R_{s2}) & 0\\ 0 & 0\end{bmatrix}$.

We choose k_1 and k_2 such that the matrices $\boldsymbol{A}$ and $\bar{\boldsymbol{A}}$ are Hurwitz. Thus, there exists a symmetric positive definite matrix $\boldsymbol{P}=\boldsymbol{P}^T>0$ satisfying $\bar{\boldsymbol{A}}^T\boldsymbol{P}+\boldsymbol{P}\bar{\boldsymbol{A}}=-\boldsymbol{I}_6$. Consider a Lyapunov function $V_1=\boldsymbol{\eta}^T\boldsymbol{P}\boldsymbol{\eta}$. The time derivative of V_1 along the system (48) is

$$\begin{aligned}\dot{V}_1=&\dot{\boldsymbol{\eta}}^T\boldsymbol{P}\boldsymbol{\eta}+\boldsymbol{\eta}^T\boldsymbol{P}\dot{\boldsymbol{\eta}}\\ =&\varpi\mu_3\boldsymbol{\eta}^T(\bar{\boldsymbol{A}}^T\boldsymbol{P}+\boldsymbol{P}\bar{\boldsymbol{A}})\boldsymbol{\eta}+2\mu_3\boldsymbol{\eta}^T\bar{\boldsymbol{B}}\boldsymbol{P}\boldsymbol{\eta}+2\boldsymbol{\eta}^T\boldsymbol{P}\boldsymbol{C}\\ =&-\varpi\mu_3\boldsymbol{\eta}^T\boldsymbol{\eta}+2\mu_3\boldsymbol{\eta}^T\bar{\boldsymbol{B}}\boldsymbol{P}\boldsymbol{\eta}+2\boldsymbol{\eta}^T\boldsymbol{P}\boldsymbol{C}.\end{aligned} \tag{49}$$

Using Young's inequality, we have

$$2\boldsymbol{\eta}^T\boldsymbol{P}\boldsymbol{C}\le2\lambda_{\max}(\boldsymbol{P})\|\boldsymbol{\eta}\|\|\boldsymbol{\delta}\|\le\boldsymbol{\eta}^T\boldsymbol{\eta}+(\lambda_{\max}(\boldsymbol{P})\|\boldsymbol{\delta}\|)^2 \tag{50}$$

where $\lambda_{\max}(\boldsymbol{P})$ is the maximum eigenvalue of $\boldsymbol{P}$. Then (49) becomes

$$\begin{aligned}\dot{V}_1&\le-(\varpi-1)\mu_3\boldsymbol{\eta}^T\boldsymbol{\eta}+2\mu_3\boldsymbol{\eta}^T\bar{\boldsymbol{B}}\boldsymbol{P}\boldsymbol{\eta}+\mu_3(\lambda_{\max}(\boldsymbol{P})\|\boldsymbol{\delta}\|)^2\\ &\le-M\mu_3V_1+\mu_3\zeta^2\end{aligned} \tag{51}$$

where $M=(\varpi-2\lambda_{\max}(\boldsymbol{PB})-1)/\lambda_{\max}(\boldsymbol{P}),\zeta=\lambda_{\max}(\boldsymbol{P})\Delta$. By selecting $\varpi>2\lambda_{\max}(\boldsymbol{PB})+1$ and incorporating the conclusion in [42], we can deduce that V_1 will converge to a compact set $\Theta=\{V_1|V_1\le\zeta^2/M\}$ within the predefined time:

$$\lim_{t\to t_{s3}}\|\boldsymbol{\eta}\|\le o \tag{52}$$

where $o=\sqrt{\zeta^2/\left(M\lambda_{\max}(\boldsymbol{P})\right)}$. Thus, it is concluded that $\boldsymbol{D}$ can be observed within the predefined time t_{s3}.

Step 2 : Next, consider a Lyapunov function $V_2=0.5\boldsymbol{S}^T\boldsymbol{S}$. The time derivative of V_2 can be obtained as

$$\dot{V}_2=\boldsymbol{S}^T\dot{\boldsymbol{S}}=-c_2\mu_2\boldsymbol{S}^T\boldsymbol{S}-c_3\boldsymbol{S}^T\mathbf{sign}(\boldsymbol{S})+\boldsymbol{S}^T\widetilde{\boldsymbol{D}}. \tag{53}$$

Since $\widetilde{\boldsymbol{D}}$ remains bounded within $(0,t_{s3})$, the sliding surface is also bounded within $(0,t_{s3})$. By selecting $c_3>o$, we have

$$\dot{V}_2\le-c_2\mu_2\boldsymbol{S}^T\boldsymbol{S}-(c_3-o)\textstyle\sum_{i=1}^3|s_i|\le-2c_2\mu_2V_2 \tag{54}$$

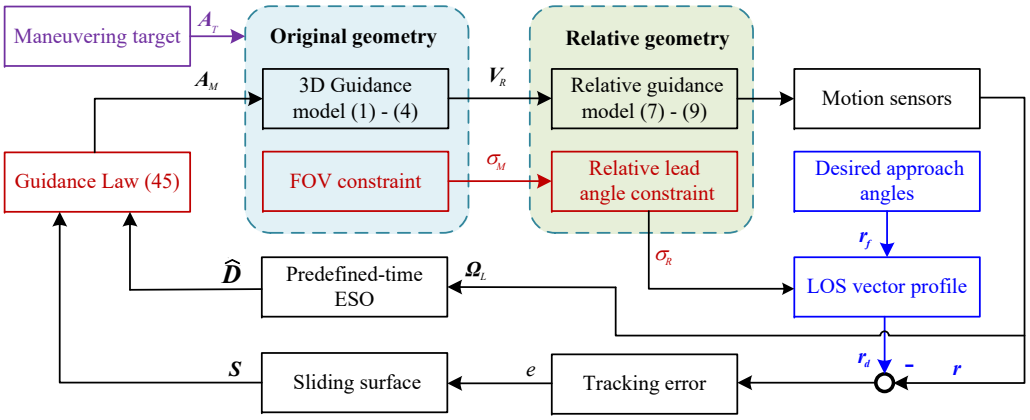

Fig. 4: Schematics of the proposed guidance law.

where $s_i, i = 1,2,3$ are the components of $\boldsymbol{S}$. Therefore, the system states will reach the sliding surface within the predefined time t_{s2} and stay on it afterwards.

When $t > t_{s2}$, substituting $\boldsymbol{S} = 0$ into (43) leads to

$$\boldsymbol{\Omega}_L - \boldsymbol{\Omega}_{Ld} = -c_1\mu_1 e\boldsymbol{k}_d. \tag{55}$$

According to (42), the tracking error dynamics can be solved as $\dot{e} = -c_1\mu_1 e$. Similar to Step 1, the tracking error can converge to zero with the settling time t_{s1}. Hence, the LOS vector profile $\boldsymbol{r}_d$ can be precisely tracked by the proposed guidance law. This completes the proof. ∎

Remark 5: Unlike finite-time control methods, the prescribed-time control technique used in this paper allows for explicit pre-assignment of t_{si}. This is an advantage of the proposed guidance law because the convergence time does not rely on initial missile states and guidance parameters. Furthermore, due to the difficulty in precisely predicting impact time for maneuvering targets, the independent variable of the scaling function is changed from the relative range R to time t. By selecting $0 < R_s < R$, the specified settling range ensures that the guidance error converges before the end of the guidance phase. Hence, the proposed guidance law is applicable to various initial conditions, without requiring a complex settling time tuning process.

Remark 6: The feasibility analysis obtained in this paper is necessary for avoiding infeasible constraints. In addition to our proposed method, barrier Lyapunov functions have also been applied to the guidance problem with FOV constraints [26], [27]. However, the nonlinear feature of Barrier Lyapunov functions makes it hard to derive an achievable guidance region analytically. Moreover, as the system state approaches the boundaries of constraints, the magnitude of Barrier Lyapunov functions will become infinite, which could potentially hinder the online implementation of guidance laws. It is worth emphasizing that the aforementioned issues are addressed by the analytical solution (31) and the feasibility analysis (39) in this paper.

B. Integrated Guidance System Framework

In practice, the missile is typically controlled by the normal acceleration in its velocity frame (X_V, Y_V, Z_V). In [35], the geometric relationship between missile acceleration $\boldsymbol{A}_M$ and relative command $\boldsymbol{A}_R^N$ has been formulated as

$$\begin{aligned} \boldsymbol{A}_R^N &= \boldsymbol{\Omega}_{\boldsymbol{V}_R} \times \boldsymbol{V}_R, \\ \boldsymbol{A}_M &= \frac{[\boldsymbol{v}_R \times (\boldsymbol{A}_R^N + \boldsymbol{A}_T)] \times \boldsymbol{v}_M}{\boldsymbol{v}_R \cdot \boldsymbol{v}_M}. \end{aligned} \tag{56}$$

Denote the unit vector along the OZ_V axis as

$$z_V = \frac{(\boldsymbol{v}_M \times z_I) \times \boldsymbol{v}_M}{\|(\boldsymbol{v}_M \times z_I) \times \boldsymbol{v}_M\|} \tag{57}$$

where z_I is the unit vector along the OZ_I axis. Then the unit coordinate vector along the OY_V axis is $\boldsymbol{y}_V = z_V \times \boldsymbol{v}_M$. If $\boldsymbol{v}_M$ and z_V have the same direction, z_V can be assigned to any unit vector lying in the horizontal plane. Then the guidance accelerations in (X_V, Y_V, Z_V) can be obtained as

$$a_{my} = \boldsymbol{y}_V \cdot \boldsymbol{A}_M, \quad a_{mz} = z_V \cdot \boldsymbol{A}_M. \tag{58}$$

It is worth noting that our guidance law can be easily extended to intercept stationary targets by setting $\boldsymbol{V}_R = \boldsymbol{V}_M$. In this situation, the proposed LOS vector shaping method needs to be implemented by simply removing the relative guidance model and the ESO, without any other modifications.

To provide a structured description of the implementation mechanism, the guidance framework is shown in Fig. 4. As previously stated, the proposed guidance law is rigorously established without the need of switching logic and linearization procedures.

V. Numerical Simulations

In this section, numerical simulations are used to showcase the performance of the FOV-limited guidance law under various constraints. All simulations initialize the target at the origin (0,0,0) km, with its trajectory shown as black curves in the figures. The speed of the missile is 320 m/s, and its normal acceleration is limited to 100 m/s^2. The parameters for the scaling functions are selected as $R_{s1} = 0.78R_0, R_{s2} = 0.8R_0, R_{s3} = 0.85R_0$, and the guidance parameters are chosen as $c_1 = 1, c_2 = 0.1, c_3 = 10^{-5}, \mu_3 = 100, k_1 = 2, k_2 = 1$, and $\varpi = 0.3$. Various terminal approach angles, FOV constraints, target maneuvers are implemented in the simulation respectively, as well as comparative simulations.

A. Performance evaluation under various approach angle constraints.

In this subsection, the performance of the proposed guidance law (45) is evaluated under various approach angles and FOV constraints. In the first group of simulations, the elevation and azimuth LOS angles are set to $-45°$ and $45°$, respectively, while the pitch and yaw lead angles are selected as $15°$ and $0°$, respectively. The speed of the target is 30 m/s, and its acceleration is by $[0, 4\sin(t/5), 0]$ m/s^2, which represents the motion pattern of a rapid sailing warship. Based on the terminal conditions and selection criteria outlined in (22), we can choose the parameters $n = [6, 9, 8.5, 7]$ and $1/\beta = [0.1, 0.18, 0.15, 0.14]$ for the LOS vector profiles. The resulting trajectories of the proposed approach angle control guidance law are shown in Fig. 5 for various desired approach angles.

Fig. 5a) and 5b) demonstrate that the proposed guidance law successfully meets the approach angle constraints in all tested scenarios. In Fig. 5c), the flight trajectories generated by the LOS vector shaping method ensure strict constraints on the FOV, keeping the lead angle within $60°$ throughout the entire flight process. It is noteworthy that the relative lead angle ultimately converges to zero. Furthermore, the acceleration command encounters no singularities throughout the entire flight and converges to bounded values at the terminal moment, as shown in Fig. 5d). Only the components for compensating target maneuvers are remained in the terminal acceleration. This is a unique feature of the proposed shaping method that greatly facilitates the online implementation of our guidance law for maneuvering targets. Additionally, we can find that the relative lead angles reach peak values at different moments, as determined by the shaping method based on parameters n and β.

B. Performance evaluation under various FOV constraints.

Next, various maximum permissible values of the FOV are selected in the second group of simulations to validate the performance of the proposed guidance law. The simulation conditions in this section are the same as in the previous. For the specified constraints in this subsection, the profile parameters are selected as $n = [7.3, 2, 7.1, 1.8]$ and $1/\beta = [0.05, 0.1, 0.1, 0.25]$. The simulation results for the proposed

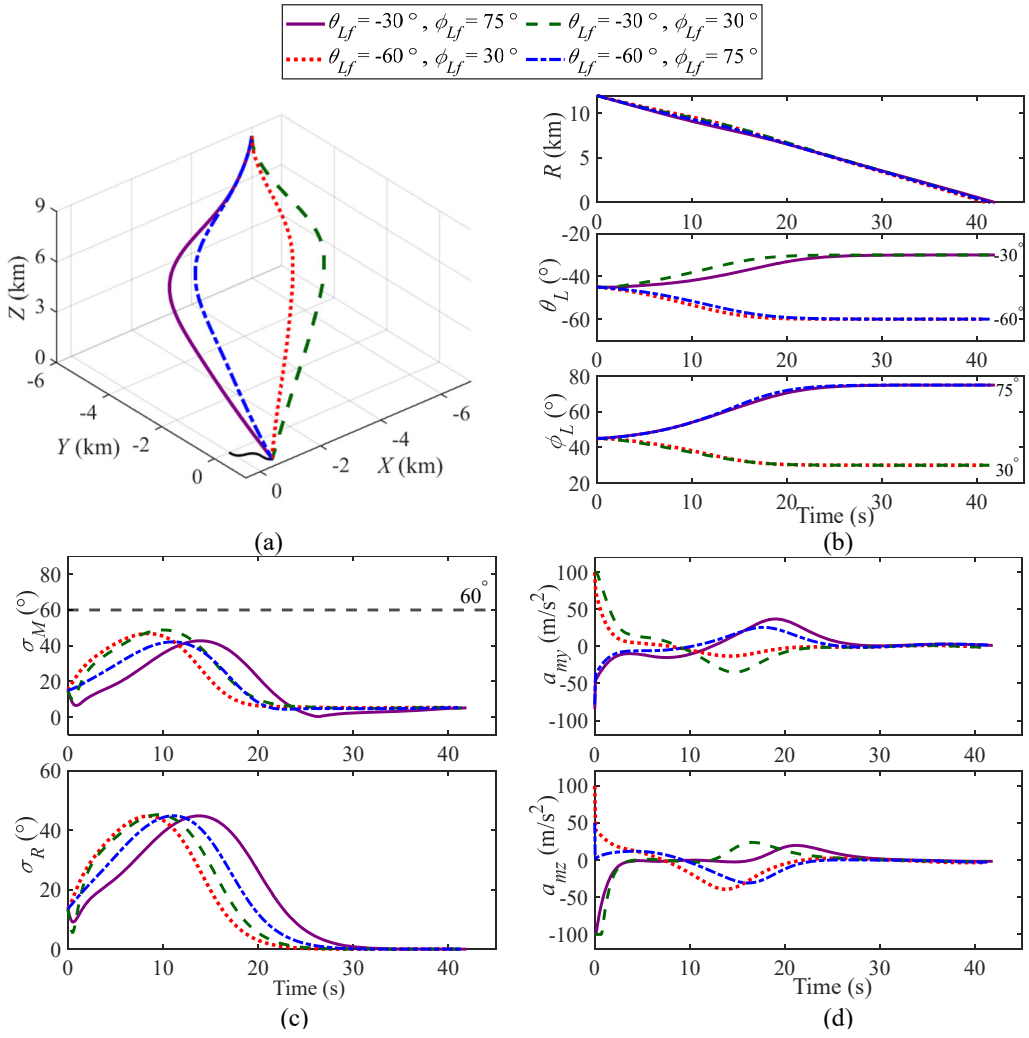

Fig. 5: Guidance law applied to various approach angle constraints. a) Flight trajectories. b) Relative ranges and approach angles. c) Lead angles and relative lead angles. d) Guidance commands.

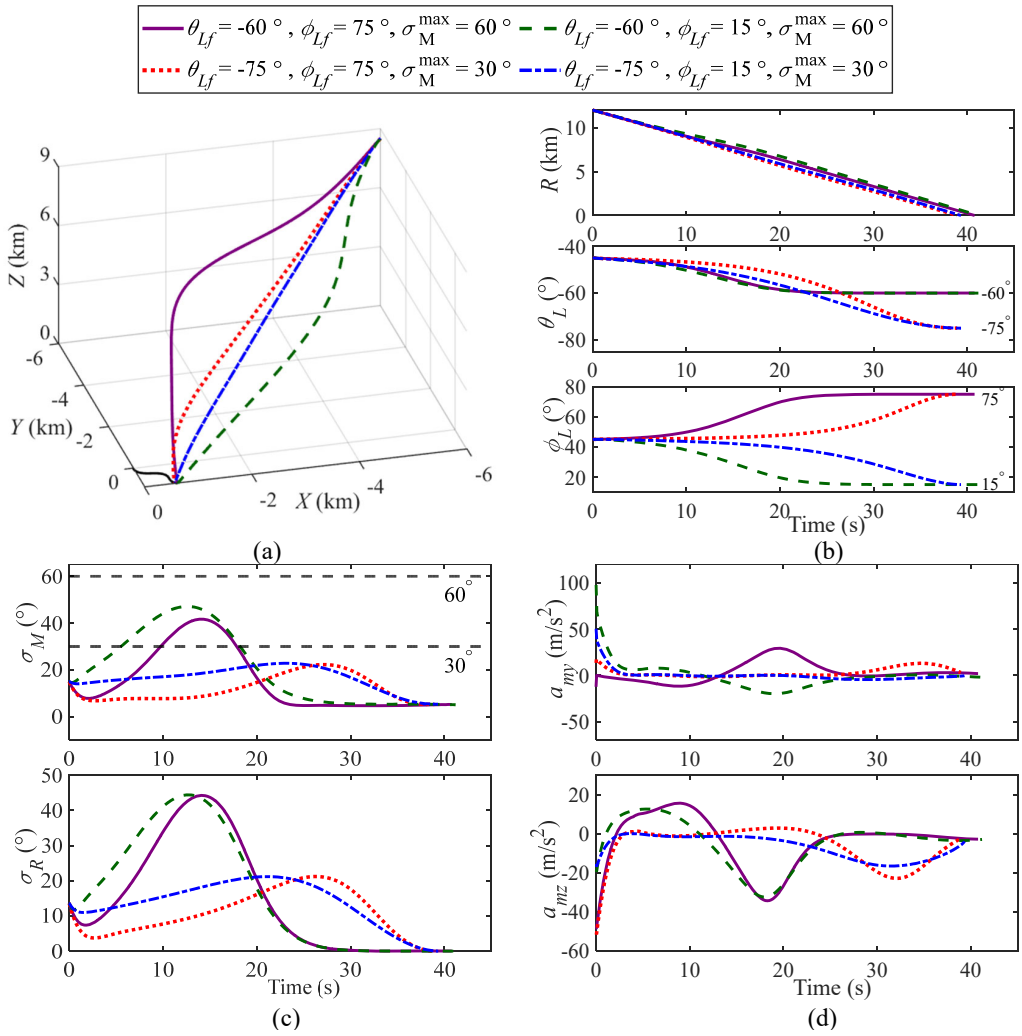

Fig. 6: Guidance law applied to various FOV constraints and desired approach angles. a) Flight trajectories. b) Relative ranges and approach angles. c) Lead angles and relative lead angles. d) Guidance commands.

guidance law under various FOV constraints are presented in Fig. 6.

Figures 6a) and 6b) illustrate that the missiles not only successfully intercept the target but also satisfy the imposed guidance constraints. As depicted in Fig. 6, the maximum lead angles for the third and fourth simulation cases (dotted line and dash-dot line) are limited to 30°, resulting in straighter flight trajectories. In contrast, the first and second simulation cases, with a maximum lead angle of 60°, generate more curved flight trajectories. Figures 6b) and 6c) demonstrate that the proposed guidance law achieves approach angle control and FOV constraints despite the unknown target maneuvers. Owing to the safety margin demonstrated in Remark 2, the peak lead angle in Fig. 6c) does not closely approach the upper boundary. This highlights the unique property of our guidance law in managing the FOV constraint against maneuvering targets.

We also need to pay attention to the terminal values of the generated acceleration commands. Both Figs. 5d) and 6d) demonstrate that all acceleration commands do not exhibit any singularity issues as the relative range R approaches zero. At the impact moment, the acceleration curves of the missiles under different conditions coincide at the same value, which precisely reflects the component induced by the target maneuvers. This stands as a significant advantage of our guidance law that other studies have not achieved.

C. Performance evaluation under various target maneuvers.

This section validates the performance of the proposed guidance law under a variety of maneuvering targets. The simulation conditions for various target maneuvers and speeds are summarized in Table I. The terminal approach angle constraints are fixed as $\theta_{Lf} = -60°$ and $\phi_{Lf} = 30°$, while the FOV constraint is set to 45°. The profile parameters are designated as $n = 3.5$ and $1/\beta = 0.4$, respectively. Simulation results are illustrated in Fig. 7, where the black curves denote trajectories generated by different target maneuvers.

In Fig. 7, all missiles intercept the targets with desired terminal approach angles under different target maneuvers. It is clearly shown in Fig. 7c) that there is always a safety margin between the actual lead angle and the maximum permissible value, regardless of the target's maneuvers. From Fig. 7c) and 7d) we can observe that the proposed guidance law

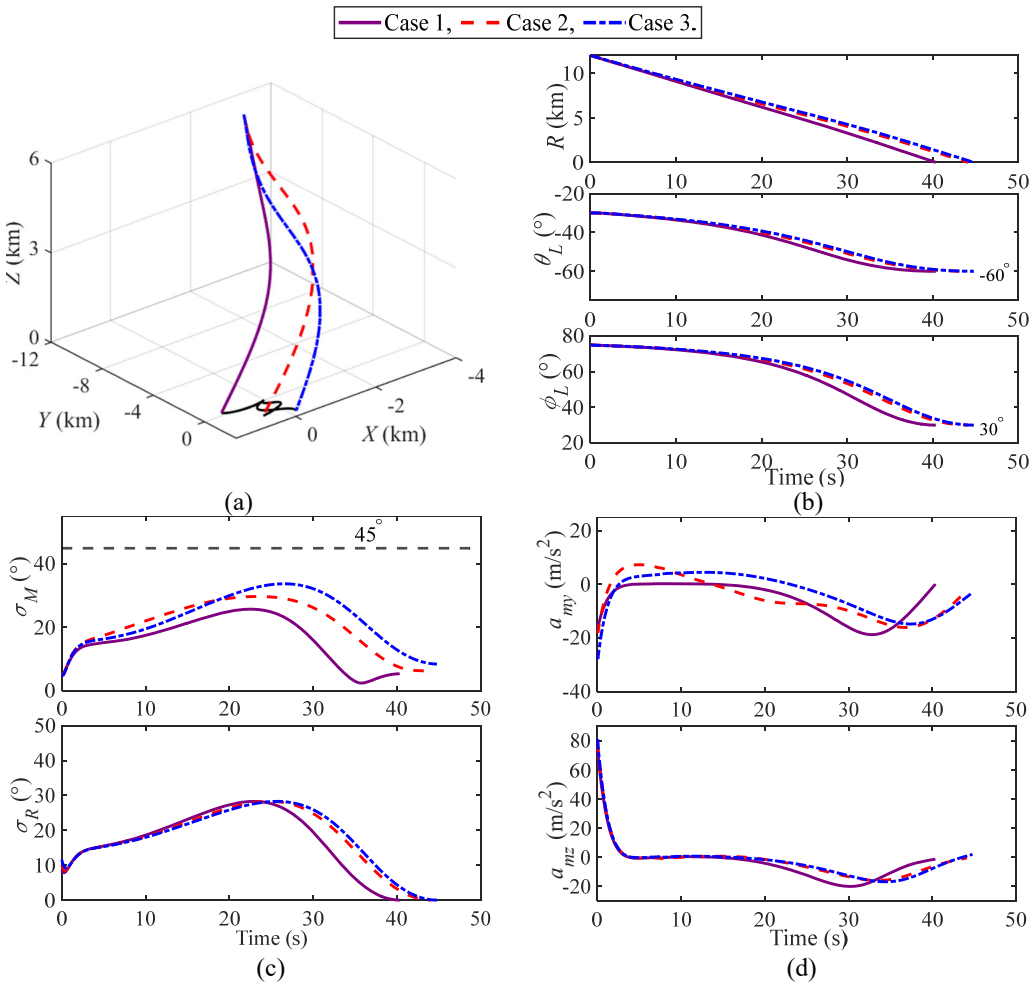

Fig. 7: Guidance law applied to various target maneuvers. a) Flight trajectories. b) Relative ranges and approach angles. c) Lead angles and relative lead angles. d) Guidance commands.

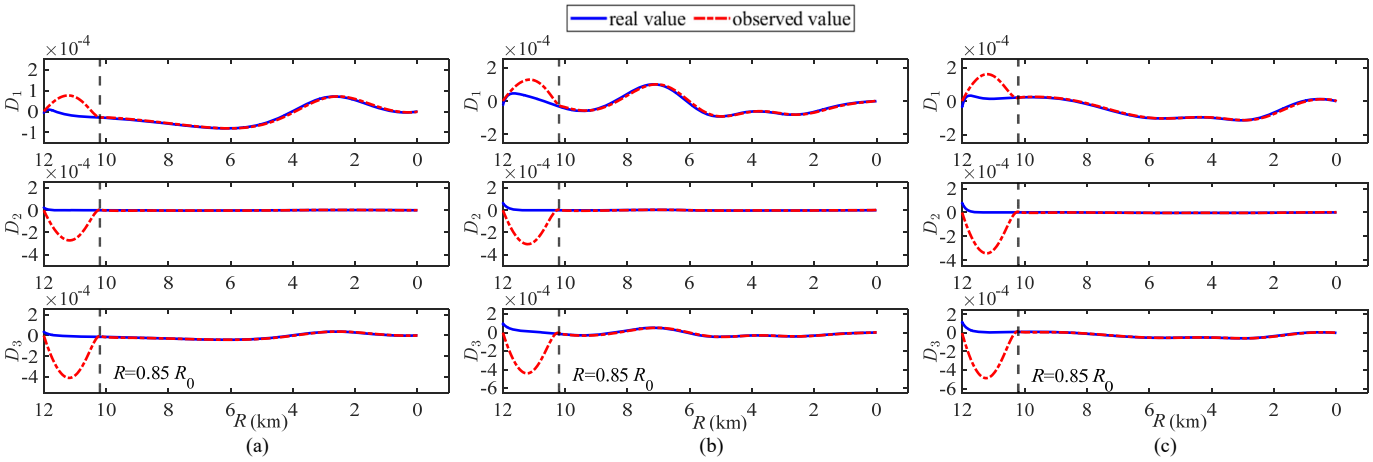

Fig. 8: Simulation results of the predefined-time ESO. a) Perturbation term of Case 1. b) Perturbation term of Case 2. c) Perturbation term of Case 3.

achieves the zero terminal relative lead angle and bounded terminal guidance command for all simulation cases. These results demonstrate that the proposed method exhibits excellent robustness against maneuvering targets.

In addition, the simulation results depicted in Fig. 8 illustrate the performance of the designed predefined-time ESO. Notably, the estimation errors for different target maneuvers converge to a neighborhood of zero when $R = R_s$. For all simulation cases, the settling range R_s was set to a same value, which ensures the convergence of observer errors and avoids the complexity of parameter tuning. These simulation results emphasize the effectiveness of the designed LOS shaping

TABLE I: Simulations Cases

Simulation case	Target acceleration (m/s^2)	Target speed (m/s)
Case 1	$[0, 4\sin(t/9), 0]$	30
Case 2	$[0, 4\cos(t/9)+3\sin(t/4), 0]$	40
Case 3	$[0, -1.5, 0]$	50

method and the predefined-time ESO-based guidance law in intercepting maneuvering targets.

D. Comparison Study.

To further demonstrate the superiority of our proposed method, this section conducts two groups of comparative simulations. As mentioned earlier, there are few existing studies on FOV-limited approach angle control guidance for 3D maneuvering targets. Therefore, in the first group of comparative simulations, our method is compared with the guidance law in [21] and [22] under stationary target condition. Furthermore, the second group of comparative simulations compares our method with the guidance law in [30] and [35] for a maneuvering target. As previously stated, vector guidance can serve as a unified tool for intercepting stationary and maneuvering targets. Therefore, by setting $\boldsymbol{V}_R = \boldsymbol{V}_M$ and removing the ESO, the guidance law proposed in this paper for maneuvering targets can be directly applied to stationary targets.

The comparative results in Fig. 9 demonstrate that all missile realize the desired terminal conditions for stationary targets and adhere to the lead angle constraint. A notable characteristic of the guidance law in [22] is that the lead angle approaches the constraint boundary early in the guidance initiation phase, resulting in the saturation of the initial acceleration command. On the other hand, the guidance law in [21] yields the smallest value of lead angle and acceleration commands under identical conditions. However, the convergence speed of the approach angle error in [21] is relatively slow, which may affect the terminal performance of the guidance system. Our guidance law does not exhibit the aforementioned issues and yields a smoother lead angle profile compared to the method proposed in [22].

Finally, the comparative simulation results of the proposed guidance law with those in [30] and [35] are presented in

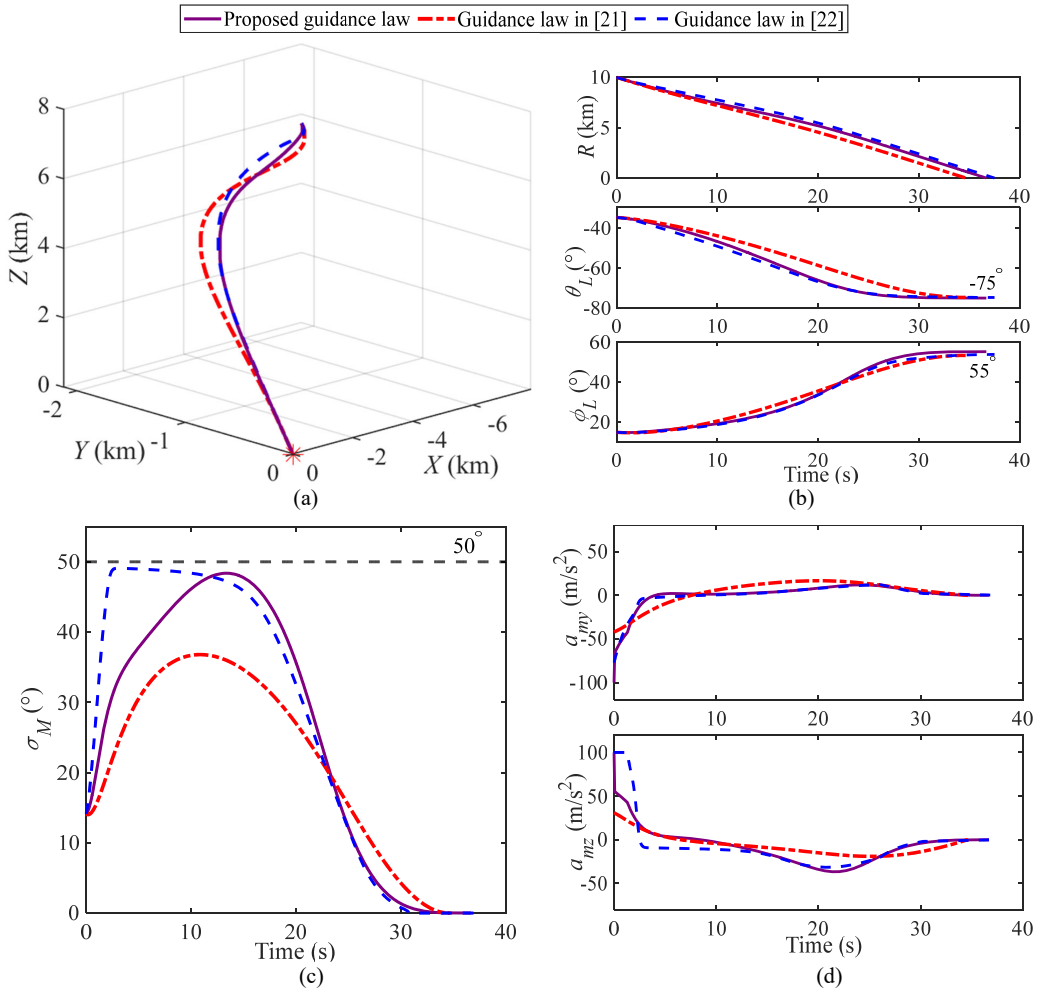

Fig. 9: Comparison study with guidance laws in [21] and [22] against stationary targets. a) Flight trajectories. b) Relative ranges and approach angles. c) Lead angles. d) Guidance commands.

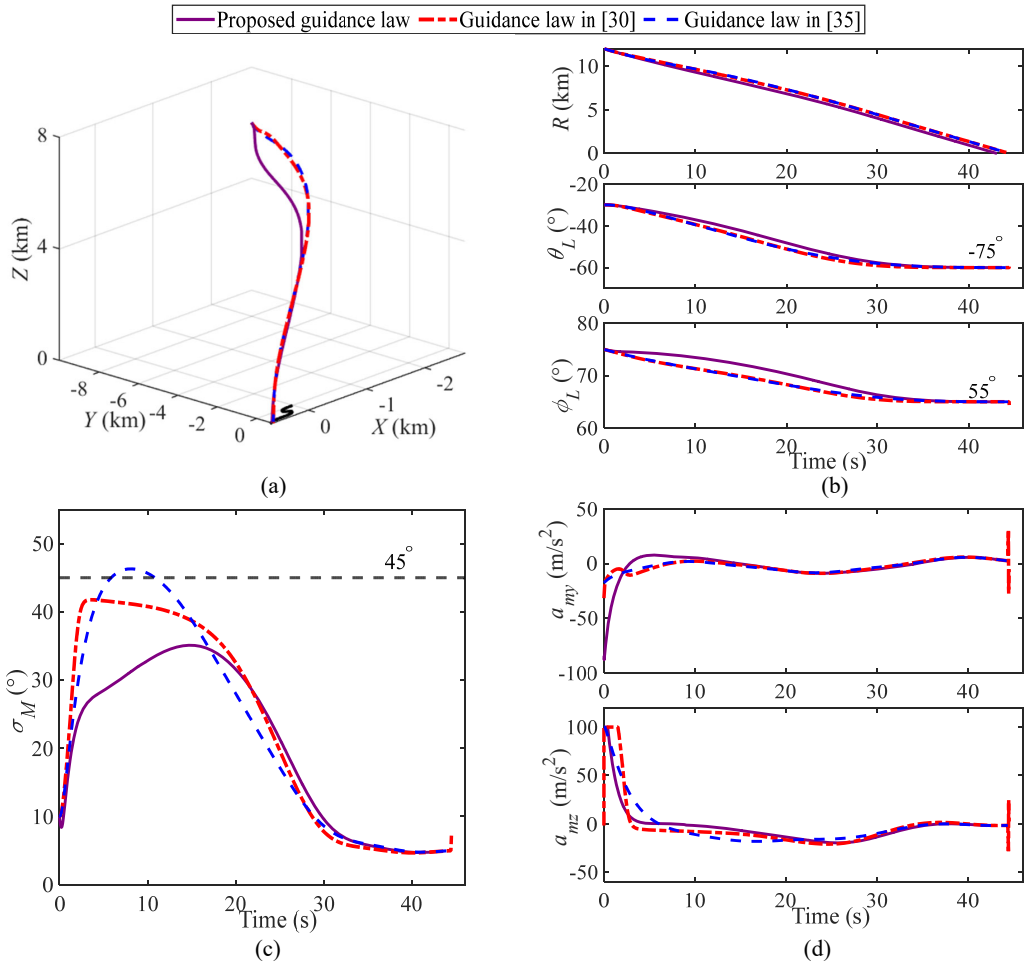

Fig. 10: Comparison study with guidance laws in [30] and [35] against maneuvering targets. a) Flight trajectories. b) Relative ranges and approach angles. c) Lead angles. d) Guidance commands.

Fig. 10. It can be observed from Fig. 10b) and 10c) that the proposed guidance law achieves the FOV constraint and the approach angle control, and its relative lead angle converges to zero before the end of guidance. However, the terminal command singularities generated by the guidance law in [30] may degrade the impact accuracy. Additionally, the nonlinear mapping method used in [30] makes it challenging to derive an analytical achievable region. Since the guidance law in [35] does not impose the FOV constraint, the resulting lead angles exceed the upper bound of 45°, as shown in Fig. 10c). Admittedly, the guidance law in [35] can satisfy the FOV constraint by tuning the guidance parameters properly. However, this complex procedure poses a challenge for mission designer in determining appropriate parameters before implementation. In contrast, the FOV-limited approach angle control guidance law proposed in this paper addresses these challenges by leveraging the achievable region outlined in (39).

VI. Conclusion

A 3D vector guidance law for missiles was proposed to achieve approach angle control with FOV constraints. First, a relative coordinate system was used to transform the FOV constraint into a limit on the relative lead angle. The zero missile distance, FOV constraint, and desired approach angles were achieved by guiding the missile to track a unit LOS vector profile accurately. Second, a guidance law was designed using prescribed-time control for capturing maneuvering targets. The closed-loop stability of the guidance was rigorously proven using Lyapunov functions. Finally, extensive numerical simulations demonstrated the efficacy and superior performance of the proposed guidance law. Unlike most existing studies, the proposed guidance law and feasibility analysis do not rely on switching logic and linearization procedures. A future study is needed to investigate how to apply the proposed vector guidance to the 3D impact time control problem for maneuvering targets.

Appendix A
Proof of Lemma 1

Similar to σ_R, the following relationships can be derived

$$\cos\sigma_M = \boldsymbol{r}\cdot\boldsymbol{v}_M,\ \sin\sigma_M\boldsymbol{k}_M = \boldsymbol{r}\times\boldsymbol{v}_M. \tag{A1}$$

$$\cos\sigma_T = \boldsymbol{r}\cdot\boldsymbol{v}_T,\quad \sin\sigma_T\boldsymbol{k}_T = \boldsymbol{r}\times\boldsymbol{v}_T. \tag{A2}$$

From the definition of $\boldsymbol{V}_R$, we obtain:

$$\begin{aligned}\boldsymbol{r}\times\boldsymbol{v}_M &= \boldsymbol{r}\times(\boldsymbol{V}_R+\boldsymbol{V}_T)/V_M\\ &= V_R/V_M\boldsymbol{r}\times\boldsymbol{v}_R + V_T/V_M\boldsymbol{r}\times\boldsymbol{v}_T.\end{aligned} \tag{A3}$$

Substituting (12), (A1), and (A2) into (A3) gives

$$\rho_R \sin\sigma_R \boldsymbol{k}_R + \rho_M \sin\sigma_T \boldsymbol{k}_T = \sin\sigma_M \boldsymbol{k}_M \tag{A4}$$

where $\rho_R = V_R/V_M$. To satisfy the FOV constraint, the following condition must hold:

$$\|\rho_R \sin\sigma_R \boldsymbol{k}_R + \rho_M \sin\sigma_T \boldsymbol{k}_T\| < \sin\sigma_M^{\max}. \tag{A5}$$

Using the triangle inequality, the following condition is required to satisfy (A5):

$$\|\rho_R \sin\sigma_R \boldsymbol{k}_R\| + \|\rho_M \sin\sigma_T \boldsymbol{k}_T\| < \sin\sigma_M^{\max}. \tag{A6}$$

To ensure (A6), the following condition is necessary

$$\|\rho_R \sin\sigma_R \boldsymbol{k}_R\| + \rho_M < \sin\sigma_M^{\max}. \tag{A7}$$

Equation (A7) is equivalent to

$$\|\sin\sigma_R\| < \frac{\sin\sigma_M^{\max} - \rho_M}{\rho_R}. \tag{A8}$$

From $V_R = V_M\sqrt{1+\rho_M^2 - 2\rho_M \boldsymbol{V}_M\cdot\boldsymbol{V}_T}$, we have $\rho_R \in (1-\rho_M, 1+\rho_M)$. Thus, a sufficient condition for the above equation can be obtained as

$$\|\sin\sigma_R\| < \frac{\sin\sigma_M^{\max} - \rho_M}{1+\rho_M}. \tag{A9}$$

Let $\sigma_R^{\max} = \operatorname{asin}(\sin\sigma_M^{\max} - \rho_M/(1+\rho_M))$. It is clear that if the relative lead angle remains smaller than $\sigma_R^{\max}$, the missile satisfies the FOV constraint. Additionally, combining (A4) and (A6) yields

$$\sigma_M \le \operatorname{asin}(\|\rho_R \sin\sigma_R \boldsymbol{k}_R\| + \|\rho_M \sin\sigma_T \boldsymbol{k}_T\|) < \sigma_M^{\max} \tag{A10}$$

where equality holds if and only if $\rho_M = 0$, i.e., $V_T = 0$. This provides a safety margin between the actual lead angle and its upper bounds, representing a key advantage of the proposed guidance law. Lemma 1 is proven. ∎

Appendix B
Derivation of the Error Dynamics

Differentiating (41) with respect to time, we have

$$-\dot{e}\sin e = \dot{\boldsymbol{r}}_d\cdot\boldsymbol{r} + \boldsymbol{r}_d\cdot\dot{\boldsymbol{r}}, \tag{B1}$$

$$\dot{e}\cos e\boldsymbol{k}_d + \sin e\dot{\boldsymbol{k}}_d = \dot{\boldsymbol{r}}_d\times\boldsymbol{r} + \boldsymbol{r}_d\times\dot{\boldsymbol{r}}. \tag{B2}$$

According to (23) we have

$$\dot{\boldsymbol{r}}_d = -\dot{\vartheta}(\boldsymbol{r}_0\sin\vartheta + \boldsymbol{k}_f\times\boldsymbol{r}_0\cos\vartheta) = \boldsymbol{\Omega}_{Ld}\times\boldsymbol{r}_d \tag{B3}$$

where $\boldsymbol{\Omega}_{Ld} = -\dot{\vartheta}\boldsymbol{k}_f$. Substituting (8) and (B3) into (B1) yields

$$\begin{aligned} -\dot{e}\sin e &= (\boldsymbol{\Omega}_{Ld}\times\boldsymbol{r}_d)\cdot\boldsymbol{r} + \boldsymbol{r}_d\cdot(\boldsymbol{\Omega}_L\times\boldsymbol{r}) \\ &= \boldsymbol{\Omega}_{Ld}\cdot(\boldsymbol{r}_d\times\boldsymbol{r}) + \boldsymbol{\Omega}_L\cdot(\boldsymbol{r}\times\boldsymbol{r}_d) \\ &= -(\boldsymbol{\Omega}_L - \boldsymbol{\Omega}_{Ld})\cdot(\boldsymbol{r}_d\times\boldsymbol{r}). \end{aligned} \tag{B4}$$

Combining the above equation with (41), we find

$$\dot{e} = (\boldsymbol{\Omega}_L - \boldsymbol{\Omega}_{Ld})\cdot\boldsymbol{k}_d. \tag{B5}$$

Similarly, substituting (8) and (B3) into (B2) leads to

$$\begin{aligned} &\dot{e}\cos e\boldsymbol{k}_d + \sin e\dot{\boldsymbol{k}}_d \\ &= (\boldsymbol{\Omega}_{Ld}\times\boldsymbol{r}_d)\times\boldsymbol{r} + \boldsymbol{r}_d\times(\boldsymbol{\Omega}_L\times\boldsymbol{r}) \\ &= (\boldsymbol{r}\cdot\boldsymbol{\Omega}_{Ld})\boldsymbol{r}_d - (\boldsymbol{r}\cdot\boldsymbol{r}_d)\boldsymbol{\Omega}_{Ld} + (\boldsymbol{r}_d\cdot\boldsymbol{r})\boldsymbol{\Omega}_L - (\boldsymbol{r}_d\cdot\boldsymbol{\Omega}_L)\boldsymbol{r} \\ &= (\boldsymbol{\Omega}_L - \boldsymbol{\Omega}_{Ld})(\boldsymbol{r}\cdot\boldsymbol{r}_d) + (\boldsymbol{r}\cdot\boldsymbol{\Omega}_{Ld})\boldsymbol{r}_d - (\boldsymbol{r}_d\cdot\boldsymbol{\Omega}_L)\boldsymbol{r}. \end{aligned} \tag{B6}$$

Since $\boldsymbol{r}_d \perp \boldsymbol{\Omega}_{Ld}$ and $\boldsymbol{r}\perp\boldsymbol{\Omega}_L$, we have $-(\boldsymbol{r}_d\cdot\boldsymbol{\Omega}_{Ld})\boldsymbol{r} = 0$ and $(\boldsymbol{r}\cdot\boldsymbol{\Omega}_L)\boldsymbol{r}_d = 0$. We can insert these into (B6) as follows:

$$\begin{aligned} &\dot{e}\cos e\boldsymbol{k}_d + \sin e\dot{\boldsymbol{k}}_d \\ &= (\boldsymbol{\Omega}_L - \boldsymbol{\Omega}_{Ld})(\boldsymbol{r}\cdot\boldsymbol{r}_d) + (\boldsymbol{\Omega}_L + \boldsymbol{\Omega}_{Ld})\times(\boldsymbol{r}_d\times\boldsymbol{r}). \end{aligned} \tag{B7}$$

We can rearrange (B7) using (B5) as

$$\begin{aligned} \dot{\boldsymbol{k}}_d &= ((\boldsymbol{\Omega}_L - \boldsymbol{\Omega}_{Ld}) - (\boldsymbol{\Omega}_L - \boldsymbol{\Omega}_{Ld})\cdot\boldsymbol{k}_d\boldsymbol{k}_d)\cot e \\ &\quad + (\boldsymbol{\Omega}_L + \boldsymbol{\Omega}_{Ld})\times\boldsymbol{k}_d \\ &= \boldsymbol{k}_d\times((\boldsymbol{\Omega}_L - \boldsymbol{\Omega}_{Ld})\times\boldsymbol{k}_d)\cot e + (\boldsymbol{\Omega}_L + \boldsymbol{\Omega}_{Ld})\times\boldsymbol{k}_d \\ &= \boldsymbol{\Omega}_{k_d}\times\boldsymbol{k}_d \end{aligned} \tag{B8}$$

where $\boldsymbol{\Omega}_{k_d} = \boldsymbol{\Omega}_L + \boldsymbol{\Omega}_{Ld} - (\boldsymbol{\Omega}_L - \boldsymbol{\Omega}_{Ld})\times\boldsymbol{k}_d\cot e$. This completes the derivation of the error dynamics. ∎

References

[1] C.-K. Ryoo, H. Cho, and M.-J. Tahk, "Time-to-go weighted optimal guidance with impact angle constraints," *IEEE Transactions on Control Systems Technology*, vol. 14, no. 3, pp. 483–492, 2006.

[2] K. S. Erer and O. Merttopçuoglu, "Indirect impact-angle-control against stationary targets using biased pure proportional navigation," *Journal of Guidance, Control, and Dynamics*, vol. 35, no. 2, pp. 700–704, 2012.

[3] H. Kang, P. Wang, C.-H. Lee, and S. Song, "Impact time and angle guidance considering aerodynamic drag," *Journal of the Franklin Institute*, vol. 361, no. 6, 2024, Art. no. 106735.

[4] A. Ratnoo, "Nonswitching guidance law for trajectory shaping control," *Journal of Guidance, Control, and Dynamics*, vol. 40, no. 10, pp. 2721–2728, 2017.

[5] C.-K. Ryoo, H. Cho, and M.-J. Tahk, "Optimal guidance laws with terminal impact angle constraint," *Journal of Guidance, Control, and Dynamics*, vol. 28, no. 4, pp. 724–732, 2005.

[6] P. Wang, Y. Guo, G. Ma, C.-H. Lee, and B. Wie, "New look-angle tracking guidance strategy for impact time and angle control," *Journal of Guidance, Control, and Dynamics*, vol. 45, no. 3, pp. 545–557, 2022.

[7] P. Wang, C.-H. Lee, N. Cho, and B. Wie, "Generalized time-to-go inversion guidance with impact time and angle constraints," *Journal of Guidance, Control, and Dynamics*, pp. 1–20, 2024.

[8] M.-G. Seo, C.-H. Lee, and M.-J. Tahk, "New design methodology for impact angle control guidance for various missile and target motions," *IEEE Transactions on Control Systems Technology*, vol. 26, no. 6, pp. 2190–2197, 2018.

[9] H.-G. Kim and H. J. Kim, "All-aspect guidance with impact angle constraint against unknown target maneuver," *IEEE Transactions on Aerospace and Electronic Systems*, vol. 55, no. 2, pp. 830–845, 2019.

[10] S. He, D. Lin, and J. Wang, "Integral global sliding mode guidance for impact angle control," *IEEE Transactions on Aerospace and Electronic Systems*, vol. 55, no. 4, pp. 1843–1849, 2019.

[11] Q. Hu, T. Han, and M. Xin, "Three-dimensional guidance for various target motions with terminal angle constraints using twisting control," *IEEE Transactions on Industrial Electronics*, vol. 67, no. 2, pp. 1242–1253, 2020.

[12] T. Han, H.-S. Shin, Q. Hu, A. Tsourdos, and M. Xin, "Differentiator-based incremental three-dimensional terminal angle guidance with enhanced robustness," *IEEE Transactions on Aerospace and Electronic Systems*, vol. 58, no. 5, pp. 4020–4032, 2022.

[13] W. Li, Y. Song, L. Cheng, and S. Gong, "Closed-loop deep neural network optimal control algorithm and error analysis for powered landing under uncertainties," *Astrodynamics*, vol. 7, no. 2, pp. 211–228, 2023.

[14] G. Sun, M. Zhou, and X. Jiang, "Non-cooperative spacecraft proximity control considering target behavior uncertainty," *Astrodynamics*, vol. 6, no. 4, pp. 399–411, 2022.

[15] J.-H. Kim, S.-S. Park, K.-K. Park, and C.-K. Ryoo, "Quaternion based three-dimensional impact angle control guidance law," *IEEE Transactions on Aerospace and Electronic Systems*, vol. 57, no. 4, pp. 2311–2323, 2021.
[16] A. Ratnoo, "Analysis of two-stage proportional navigation with heading constraints," *Journal of Guidance, Control, and Dynamics*, vol. 39, no. 1, pp. 156–164, 2016.
[17] Y. Chen, D. Guo, J. Wang, J. Shan, and M. Xin, "Cooperative circular guidance with nonuniform field-of-view constraints," *Journal of Guidance, Control, and Dynamics*, vol. 45, no. 8, pp. 1435–1450, 2022.
[18] S. Lee, N. Cho, and Y. Kim, "Impact-time-control guidance strategy with a composite structure considering the seeker's field-of-view constraint," *Journal of Guidance, Control, and Dynamics*, vol. 43, no. 8, pp. 1566–1574, 2020.
[19] H.-G. Kim, J.-Y. Lee, H. J. Kim, H.-H. Kwon, and J.-S. Park, "Look-angle-shaping guidance law for impact angle and time control with field-of-view constraint," *IEEE Transactions on Aerospace and Electronic Systems*, vol. 56, no. 2, pp. 1602–1612, 2020.
[20] T. Han, Q. Hu, and M. Xin, "Three-dimensional approach angle guidance under varying velocity and field-of-view limit without using line-of-sight rate," *IEEE Transactions on Systems, Man, and Cybernetics: Systems*, vol. 52, no. 11, pp. 7148–7159, 2022.
[21] Q. Hu, T. Han, and M. Xin, "Analytical solution for nonlinear three-dimensional guidance with impact angle and field-of-view constraints," *IEEE Transactions on Industrial Electronics*, vol. 68, no. 4, pp. 3423–3433, 2021.
[22] J. Wang, X. Ding, Y. Chen, C. Wang, and M. Xin, "Field-of-view constrained three-dimensional impact angle control guidance for speed-varying missiles," *IEEE Transactions on Aerospace and Electronic Systems*, vol. 58, no. 5, pp. 3992–4003, 2022.
[23] P. Wang, C.-H. Lee, Y. Liu, and M.-J. Tahk, "Nonlinear three-dimensional guidance for impact time and angle control with field-of-view constraint," *IEEE Transactions on Aerospace and Electronic Systems*, vol. 60, no. 1, pp. 264–279, 2024.
[24] H. Hong, R. Tekin, and F. Holzapfel, "Guaranteed smooth trajectory generation for field-of-view constrained impact-time control," *Journal of Guidance, Control, and Dynamics*, vol. 44, no. 4, pp. 898–904, 2021.
[25] H. Hong, L. Liu, F. Holzapfel, and G. Sachs, "Dynamic soaring under different atmospheric stability conditions," *Journal of Guidance, Control, and Dynamics*, vol. 46, no. 5, pp. 970–977, 2023.
[26] X. Wang, Y. Zhang, and H. Wu, "Sliding mode control based impact angle control guidance considering the seeker's field-of-view constraint," *ISA Transactions*, vol. 61, pp. 49–59, 2016.
[27] B. Liu, M. Hou, and D. Feng, "Nonlinear mapping based impact angle control guidance with seeker's field-of-view constraint," *Aerospace Science and Technology*, vol. 86, pp. 724–736, 2019.
[28] H.-G. Kim and H. J. Kim, "Field-of-view constrained guidance law for a maneuvering target with impact angle control," *IEEE Transactions on Aerospace and Electronic Systems*, vol. 56, no. 6, pp. 4974–4983, 2020.
[29] S. Lee and Y. Kim, "Capturability of impact-angle control composite guidance law considering field-of-view limit," *IEEE Transactions on Aerospace and Electronic Systems*, vol. 56, no. 2, pp. 1077–1093, 2020.
[30] Q. Shi, H. Wang, and H. Cheng, "Multiple constraints-based adaptive three-dimensional back-stepping sliding mode guidance law against a maneuvering target," *Aerospace*, vol. 9, no. 12, 2022.
[31] P. Surve, A. Maity, and S. R. Kumar, "Polynomial shaping based three-dimensional impact angle and field-of-view constrained guidance," *Aerospace Science and Technology*, vol. 147, 2024, Art. no. 109018.
[32] C.-H. Lee, T.-H. Kim, and M.-J. Tahk, "Interception angle control guidance using proportional navigation with error feedback," *Journal of Guidance, Control, and Dynamics*, vol. 36, pp. 1556–1561, 2013.
[33] N. Cho, S. Lee, H.-S. Shin, and T.-H. Kim, "Three-dimensional biased proportional navigation guidance based on spatial rotation of predicted final velocity," *IEEE Transactions on Aerospace and Electronic Systems*, vol. 59, no. 2, pp. 1354–1370, 2023.
[34] H. Li, J. Wang, S. He, and C.-H. Lee, "Nonlinear optimal impact-angle-constrained guidance with large initial heading error," *Journal of Guidance, Control, and Dynamics*, vol. 44, no. 9, pp. 1663–1676, 2021.
[35] H. Li, J. Wang, S. He, and C.-H. Lee, "Nonlinear optimal 3-d impact-angle-control guidance against maneuvering targets," *IEEE Transactions on Aerospace and Electronic Systems*, vol. 58, no. 3, pp. 2467–2481, 2022.
[36] K. S. Erer, R. Tekin, and H. Hong, "Computational impact-time guidance with biased proportional navigation," *Journal of Guidance, Control, and Dynamics*, vol. 47, no. 6, pp. 1249–1255, 2024.
[37] R. Tekin, "Augmented plane pursuit for impact-angle control in three dimensions," *Journal of Guidance, Control, and Dynamics*, vol. 45, no. 9, pp. 1769–1775, 2022.
[38] R. Tekin and K. S. Erer, "Switched-gain guidance for impact angle control under physical constraints," *Journal of Guidance, Control, and Dynamics*, vol. 38, no. 2, pp. 205–216, 2015.
[39] W. Dong, C. Wang, J. Liu, J. Wang, and M. Xin, "Three-dimensional vector guidance law with impact time and angle constraints," *Journal of the Franklin Institute*, vol. 360, no. 2, pp. 693–718, 2023.
[40] W. Dong, F. Deng, C. Wang, J. Wang, and M. Xin, "Three-dimensional spatial–temporal cooperative guidance without active speed control," *Journal of Guidance, Control, and Dynamics*, vol. 46, no. 10, pp. 1981–1996, 2023.
[41] H. Li, Y. Liu, K. Li, and Y. Liang, "Analytical prescribed performance guidance with field-of-view and impact-angle constraints," *Journal of Guidance, Control, and Dynamics*, vol. 47, no. 4, pp. 728–741, 2024.
[42] Y. Song, Y. Wang, J. Holloway, and M. Krstic, "Time-varying feedback for regulation of normal-form nonlinear systems in prescribed finite time," *Automatica*, vol. 83, pp. 243–251, 2017.

Honglong Kang received the B.S. degree in intelligent science and technology from Qingdao University, Qingdao, China, in 2019. He is currently a Ph.D. candidate of the Center for Control Theory and Guidance Technology at Harbin Institute of Technology, Harbin, 150001, China. His research interests include cooperative guidance and control of flight vehicles, homing guidance and learning-based control.

Pengyu Wang (Member, IEEE) received the B.S. degree in automation from Harbin Engineering University, Harbin, China, in 2015, and the M.S. and Ph.D. degrees in control science and engineering from Harbin Institute of Technology, Harbin, in 2017 and 2022, respectively.

From 2022 to 2024, he was a Postdoctoral Researcher with the Department of Aerospace Engineering, Korea Advanced Institute of Science and Technology, Daejeon, South Korea. Since 2025, he has been with the Department of Control Science and Engineering, Harbin Institute of Technology, where he is currently an Associate Professor. His research interests include advanced guidance and control of aerospace systems, cooperative control, finite-time control, and learning-based control.

Dr. Wang is an Associate Editor for *International Journal of Aeronautical and Space Sciences*.

Shenmin Song received the Ph.D. degree in automatic control theory and application from Harbin Institute of Technology, Harbin, China, in 1996. He is currently a Professor with the Center for Control Theory and Guidance Technology, Harbin Institute of Technology, Harbin. His research interests include the guidance control of flight vehicles and intelligent control.

Robert Fonod (Senior Member, IEEE) received his Ph.D. in Automatic Control from the University of Bordeaux, France, in 2014, and his B.Sc. and M.Sc. degrees in Cybernetics from the Technical University of Košice, Slovakia, in 2009 and 2011, respectively. He also earned a Master of Computer Science (MCS) degree from the University of Illinois Urbana-Champaign (UIUC) in 2021.

He is currently a Research Associate at EPFL, Switzerland. Previously, he was a Research Scientist at the French-German Research Institute of Saint-Louis (ISL), an Assistant Professor at TU Delft, and a Postdoctoral Researcher at the Technion. He has also held visiting appointments at ESA and Thales Alenia Space. His research interests include guidance, navigation, and control (GNC) of aerospace vehicles, fault diagnosis, estimation and tracking, and the application of computer vision and machine learning to intelligent transportation systems (ITS).

Dr. Fonod is an Associate Editor for the *IEEE Transactions on Aerospace and Electronic Systems*.